Photo-Mediated Facile Synthesis of Silver Nanoparticles Using *Curcuma zanthorrhiza* Rhizome Extract and Their In Vitro Antimicrobial and Anticancer Activity

K. S. Aiswariya[1] · Vimala Jose[1]

Abstract

Plants possess unique bioactive principles justifying their multifunctional properties. In this work silver nanoparticles (AgNPs) were prepared via a photo-mediated green approach for enhanced antimicrobial and anticancer activity. The aqueous rhizome extract of *Curcuma zanthorrhiza* Roxb. (Cz) was employed as a source of reducing and capping agent for the synthesis of colloidal Cz-AgNPs. The materialization of Cz-AgNPs was identified from the surface plasmon resonance observed at 416 nm using UV–Visible spectrophotometer. The FTIR analysis of both Cz-AgNPs and plant rhizome extract revealed the as-synthesized Cz-AgNPs were capped with plant derived phytoconstituents. The crystallinity, surface morphology, hydrodynamic size and surface area of Cz-AgNPs were characterized by PXRD, HR-TEM, FESEM, DLS and BET analysis. The as-synthesized Cz-AgNPs exhibited strong antimicrobial activities against bacterial strains and plant pathogenic fungi in a dose-dependent manner. The antimicrobial activity of Cz-AgNPs was assessed using standard disc diffusion, broth microdilution assay for bacterial strains and poisoned food technique for fungal strains. The Cz-AgNPs were inhibitory to all the microbes even at the lowest concentration. The biocompatible nature of Cz-AgNPs was analyzed for hemolytic properties with human erythrocytes and promising results were observed. In addition, the cytotoxicity activity (Trypan Blue Exclusion Method) on the cell lines of Dalton's Lymphoma Ascites (DLA) and Ehrlich Ascites Carcinoma (EAC) showed Cz-AgNPs exhibited potential anticancer activity with concentration as low as 1.67 μg/mL and 1.84 μg/mL respectively (IC_{50} value). This work attempted at optimizing a safe dosage of silver nanoparticles using hemolysis assay and thus for application in therapy.

✉ Vimala Jose
vimalajoseparaemackel@gmail.com

1   Centre for Bionanotechnology, Research and Post Graduate Department of Botany, St. Thomas' College, University of Calicut, Thrissur, Kerala 680001, India

Graphic Abstract
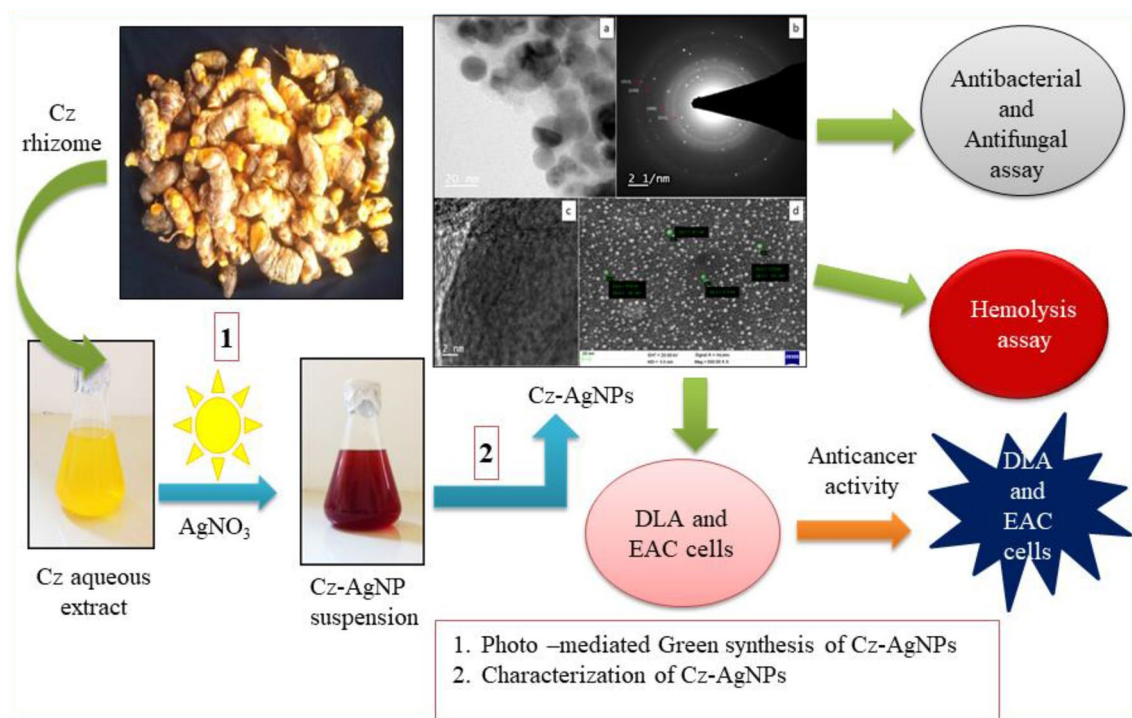
Keywords Aqueous rhizome extract · Face centered cubic structure · MIC · Hemolysis · Cytotoxicity

1 Introduction

Nanoparticles (NPs) have revolutionized the fields of materials science and medicine. They are exploited in the realms of catalysis [1], sensor technology [2], site specific drug delivery [3], imaging and cancer treatments [4]. Unfortunately, the majority of physicochemical techniques employed for the synthesis of metallic nanoparticles require the use of toxic solvents. The by-products from these processes pose a serious threat to the environment [5]. Therefore, in recent times, synthesis of metal nanoparticles using natural materials such as microbes, parasites, yeast, seaweeds and plants [6] has gained considerable interest among researchers.

Natural products derived from plants have contributed enormously in the treatment of ailments. The natural products obtained from plants possess bioactive principles. They are unique to each plant which justifies their role in therapeutics as analgesic, anticancer, anti-inflammatory, antihyperglycemic and lipolytic agents. Hence, they continue to be a critical source of contemporary drugs [7]. Phytoconstituents have the potential to interact with various other compounds through a variety of chemical reactions [8]. Apart from the medicinal properties, the chelating and antibacterial capabilities of different plants and phytoplanktons are used to treat wastewater [9]. In addition, the tanning activity of plant polyphenols have been exploited in the leather industry [8]. On the other hand, their potency is inhibited due to their low hydrophilicity and stability. The natural products are mostly regarded as vulnerable drug candidates because of their requirements in high dosages and repeated administrations [10]. Despite the advantages of the biomolecules, the exploitation of the plant resources remains in a nascent stage.

Consequently, during the recent years, synthesis of plant-based functional nanoparticles has emerged as an area of investigation among the scientific community [11]. Besides, the minimal efforts involved in synthesis, the plant material integrated nanoparticles show biocompatibility and biodegradability [12]. Therefore, the green synthesized nanoparticles have been explored in the field of nanomedicine as well. They are used in bioimaging [13], cancer theranostics [12, 14], as anti-cancerous agents [15], antibacterial [6, 16], antifungal [17], antiviral, anti-inflammatory, [14], antidiabetic [18], antioxidant [19] agents and also in wound dressing [20]. In this context, synthesis and utilization of Ag and AgNP-based materials has gained interest due to its morphology, biophysical properties and stability [21]. The green synthesized silver nanoparticles

also find its application in the degradation of pesticides [22], toxic dyes [23], as environmental sensors [24], in heavy metal removal [25–27] and mosquito control [28].

However, the properties of the green synthesized nanoparticles not only depend on the phytoconstituents present in the plant but also the reaction conditions employed during the synthesis. The synthesis of metallic nanoparticles utilizing plant's concentrates has been accounted for different plants, such as *Rheum palmatum* [29], *Ficus hispida* [30], *Cinnamomum vernum* [23], *Combretum erythrophyllum* [31], *Morus indica* [32], *Eriobotrya japonica* [33], *Zingiber officianale* [34], *Sesbania grandiflora* [35], *Taraxacum officianale* [36], *Aspilia pluriseta* [37], *Caesalpinia pulcherrima* [38], *Sansevieria roxburghiana* [39]. But there is still a wide spectrum of plant metabolites which are yet to be investigated. For instance, the rhizomes of *Curcuma zanthorrhiza* Roxb. (Cz) which are rich in phenols, alkaloids, flavonoids, tannins, curcuminoids, terpenoids and xanthorhizol [40], have not been exploited so far in the synthesis of AgNPs. The presence of these secondary metabolites accounts for its medicinal properties such as diuretic, anticancer, antioxidant, antibacterial, antifungal, anti-inflammatory and hepatoprotective effects [41, 42]. Besides, *C. zanthorrhiza* is used as a cosmetic herb in South Asia [43].

Based on the above considerations, an attempt has been made in this paper to synthesize silver nanoparticles for the first time using the aqueous rhizome extract of *C. zanthorrhiza* Roxb. Further, to characterize the as-synthesized nanoparticles using different spectroscopic and electron microscopic techniques. The in vitro antibacterial, antifungal, hemolytic and cytotoxic potential of the as-synthesized silver nanoparticles (Cz-AgNPs) has also been investigated. The novelty of the present work lies in the usage of rhizome extracts of *C. zanthorrhiza*, which is a cheap, renewable and easily available resource. The results suggest the utilization of Cz-AgNPs as a promising chemotherapeutic drug.

2 Materials and Methods

2.1 Preparation of Rhizome Extract

Curcuma zanthorrhiza rhizomes (Fig. 1a) were collected from the germplasm of Regional station of National Bureau of Plant Genetic Resources (NBPGR), Thrissur, Kerala, India. Rhizomes were washed with distilled water, dried in shade, and ground into fine powder. Subsequently, 10% (w/v) aqueous rhizome extract was prepared by boiling 10 g rhizome powder in 100 mL deionized water for 30 min. Thereafter, the aqueous rhizome extract was filtered using Whatman no.1 filter paper and the filtrate was centrifuged at 5000 rpm. The supernatant thus obtained was stored at 4 °C for subsequent experiments.

2.2 Green Synthesis of Silver Nanoparticles (Cz-AgNPs)

The aqueous solution of *C. zanthorrhiza* rhizome extract was taken in Erlenmeyer flask and 1 mM silver nitrate (Sigma Aldrich) solution was added to it (in the ratio 1:10 by volume). The flask was kept under stirring in sunlight for 1 h. After an hour of stirring, silver nanoparticles (Cz-AgNPs) were obtained. The nanoparticles were separated from the solution by repeated centrifugation at 12,000 rpm (Eppendorf 5430R). Finally, they were washed with deionized water to remove the water soluble biomoieties and the nanoparticle suspension was lyophilized. The lyophilized nanoparticle suspension was used for all the further experiments.

2.3 Characterization of Cz-AgNPs

The formation of Cz-AgNPs using the aqueous plant rhizome extract as reducing agent was monitored by recording the UV-Visible spectra of the solution using UV–Visible spectrophotometer (Shimadzu UV probe 1800), at a

Fig. 1 **a** Fresh rhizomes of *C. zanthorrhiza*, **b** 10% aqueous rhizome extract of *C. zanthorrhiza* (Yellow colour), **c** Cz-AgNPs suspension formed after the addition of 1 mM AgNO₃ solution to the plant rhizome extract (Reddish brown colour), exposed to sunlight for 1 h (Color figure online)
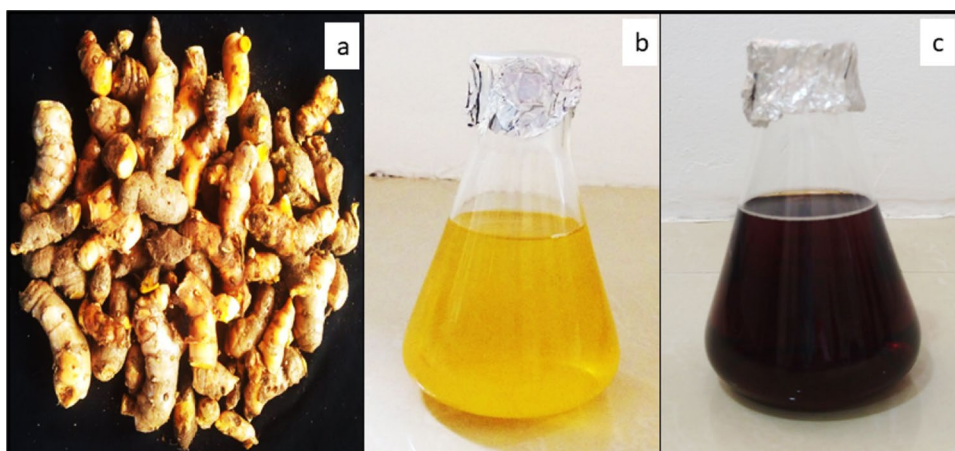
resolution of 1 nm in the scanning range 600–300 nm. The infra-red spectra of both the plant rhizome extract and Cz-AgNPs were analyzed to understand the specific functional groups in the phytochemicals which are responsible for the reduction and stabilization of nanoparticles. The Fourier Transform Infra-Red (FTIR) spectra were recorded using Thermo Nicolet, Avatar 370 FTIR spectrophotometer in the spectral range of 4000–500 cm^{-1} and resolution of 4 cm^{-1}. Powder X-ray diffraction (XRD) pattern of the Cz-AgNPs was collected on a Malvern Panalytical Aeris diffractometer using Ni-filtered CuKa radiation. The data was collected with a step size of 0.02° and count time of 2 s per step over the range $10° < 2\theta < 80°$. The average crystallite size of Cz-AgNPs was calculated using the Scherrer equation, where, $D = k\lambda/\beta 1/2 \cos\theta$ where, D = average crystallite size, k = Scherrer's constant (0.94), λ = X-ray wavelength, $\beta_{1/2}$ = pure diffraction broadening peak at half height and θ = diffraction angle. High-Resolution Transmission Electron Microscope (HR—TEM, Tecnai G2, F30) operated at 300 kV was used to examine the size, diffraction ring pattern (SAED), lattice fringes and d spacing of the as-synthesized silver nanoparticles. Further, the topography of the Cz-AgNPs was observed using Karl Zeiss FESEM Supra 55 Field Emission Scanning Electron Microscope (FESEM) operated at an accelerating voltage of 20 kV. The hydrodynamic particle size of the Cz-AgNPs was measured using Dynamic Light Scattering (DLS) technique (Horiba Scientific SZ-100). The measurement parameters included 633 nm wavelength, scattering angle of 90°, temperature of 25 °C, and dispersion medium viscosity of 0.894 mPa s. The specific area of the Cz-AgNPs was determined using the surface area and porosity analyzer (BET), Belsorp Mini 11, BEL Japan. The porosity was measured using a nitrogen adsorbent isotherm at 77 °C. Total pore volume and pore size were estimated by BJH method.

2.4 Antibacterial Activity of Cz-AgNPs

2.4.1 Disc Diffusion Method

Antibacterial activity of silver nanoparticles was analyzed using Kirby—Bauer disc-diffusion method [44] against selected bacterial strains, *Staphylococcus aureus* (MTCC96) and *Escherichia coli* (MTCC40). The pure cultures obtained from Institute of Microbial Technology, Chandigarh, India were used for the experiment. Initially, a prepared nutrient agar (Sigma-Aldrich, 28 g/L) was poured on sterile petriplates and allowed to solidify. Agar surface of each plate was then smeared with a sterile cotton swab of the selected bacterial strain. Subsequently, the sterile discs impregnated with 20 μL of various concentrations (10, 25, 50, 75, and 100 μg/mL) of Cz-AgNPs were allowed to dry in sterile conditions. Later it was placed on solidified agar plates at equal distance

along with control. Vancomycin disc (Sigma-Aldrich) was used as the positive control and a disc with deionised water served as the negative control. In addition, discs with 20 μL of 1 mM silver nitrate solution and 0.1 g/mL plant rhizome extract were also maintained. The plates (in triplicate) were then incubated at 37 ℃, and the zone of inhibition (ZOI) was measured in mm after 24 h.

2.4.2 Broth Microdilution Assay

Six serial dilutions (10^{-1}, 10^{-2}, 10^{-3}, 10^{-4}, 10^{-5}, 10^{-6} mL) of clinical isolates of *E. coli* and *S. aureus* were made using the Luria Bertani (LB) broth (Sigma-Aldrich). Thereafter 1 mL each of bacterial suspension from 10^{-5} dilution was transferred to the sterile petriplates and molten nutrient agar was added to it. The petriplates were incubated overnight, after thorough rotation. Subsequently, 4 to 5 colonies from the nutrient agar plate were inoculated into the LB broth. The culture was read at 600 nm to adjust the final inoculum to 5×10^5 cfu/mL.

For the broth microdilution test, 50 μL of each bacterial suspension (*E. coli, S. aureus*) in LB broth was added to the wells of a sterile 96-well microtitre plate which already contained 50 μL of two-fold serially diluted antibiotic (Ampicillin), Cz-AgNPs, plant rhizome extract and silver nitrate solution in LB broth medium respectively. The highest concentration of antibiotic and Cz-AgNPs was 10 mg/L. 10 mg/L solution was further diluted to 512, 256, 128, 64, 32, 16, 8, 4, 2 and 1 μg/mL and the end volume in each well was maintained at 100 μL. The wells 11 and 12 served as the growth control and sterile control, respectively. The contents of each well were mixed up and down using micropipettes before incubation for 24 h. The MIC (Minimum Inhibitory Concentration) was the lowest concentration of inoculum where no growth was observed after 24 h incubation with test solutions [45]. The respiratory activity was determined by adding 10 μL/well of TTC (2,3,5- triphenyl tetrazolium chloride, Sigma-Aldrich) dissolved in water (TTC 20 mg/mL) and incubated for 30 min in the dark [46]. The plates were read with a microplate reader (BIO-Base) at 600 nm. The wells with bacterial suspension in an appropriate growth medium served as positive control. The wells with growth medium containing plant rhizome extract served as negative control. All measurements of MIC values were repeated in triplicates.

2.5 Antifungal Activity of Cz-AgNPs

For evaluating the antifungal activity of Cz-AgNPs, poisoned food technique [47] was followed. The Potato Dextrose Agar (PDA) was prepared (HiMedia—39 g/L) and kept in molten state at 70–80 °C. One third of the petriplates were filled with this molten agar. The various concentrations of

Cz-AgNP solution (10, 25, 50, 75 and 100 μg/mL) were prepared. 2 mL of CzAgNP solution was pipetted into each plate, mixed well and allowed to solidify. A PDA plate with 2 mL each of sterile distilled water and fluconazole (100 μg/mL) served as negative and positive control respectively. Additionally, PDA plates with 2 mL of 1 mM silver nitrate solution and plant rhizome extract (0.1 g/mL) were also maintained. Inoculum discs were cut with a potato borer (4 mm diameter) from a pure culture plate of *Aspergillus niger*, obtained from Pathology division, Kerala Agricultural University, Thrissur, Kerala, India. The plug of *A. niger* with the mycelial surface facing downwards was inoculated in the centre of each agar plate. The plates were incubated at 37 °C in dark condition for 7 days and the colony diameter was measured in mm. Three replicates were maintained. The fungi toxicity of the Cz-AgNP solution in terms of percentage of inhibition of mycelial growth was calculated using the formula.

$$Percentage\ of\ inhibition\ =\ C-T/C\times100$$

where, C = Average increase in mycelial growth in the control plate (negative control). T = Average increase in the mycelial growth in the treatment plate.

2.6 Hemolysis Assay of Cz-AgNPs

Hemolysis experiments have been performed according to the method of Lin and Haynes, 2010 [48]. The fresh human blood samples used for the experiments were collected from (healthy, non-smoker) volunteers. Initially, 2 mL of the whole blood sample was added to 4 mL phosphate-buffered saline (PBS), centrifuged at 7800 rpm for 5 min at 4 °C to isolate red blood cells (RBCs). The isolated RBCs were further washed, re-suspended in 10 mL PBS and finally diluted to 20 mL with PBS. RBC suspension of 0.4 mL was exposed to 1.6 mL of varied concentrations (2, 10, 50, 100, 200 μg/mL) of Cz-AgNPs suspension in PBS (test group), 1 mM silver nitrate solution (test group), 1% saline Triton X—100 (positive control), and PBS (negative control). The samples were incubated at 37 °C. After 2, 4 and 6 h, the samples were centrifuged at 1600 rpm for 5 min and absorbance of the supernatant was read at 577 nm. The hemolytic degree was calculated using the following formula:

$$Hemolysis\ percentage\ =\ \left(Absorbance_{(test)}-Absorbance_{(negative\ control)}\right)/$$
$$\left(Absorbance_{(positive\ control)}-Absorbance_{(negative\ control)}\right)\times100\ \%$$

2.7 In Vitro Cytotoxicity Assay of Cz-AgNPs

The Dalton's Lymphoma Ascites (DLA) and Ehrlich Ascites Carcinoma (EAC) cell lines collected from the peritoneal cavity of mice were washed with Phosphate Buffer Saline (PBS). It was centrifuged at 1500 rpm for 3 min to remove the traces of blood. The DLA and EAC cell pellets were re-suspended in PBS to get a concentration of 1×10^7 cells/mL and used for cytotoxicity analysis. Trypan Blue Exclusion method was performed to evaluate the in vitro cytotoxicity assay. Approximately 1×10^6 DLA cells were distributed into test tubes containing different concentrations of Cz-AgNPs (0.2, 0.6, 0.8, 1, 1.6 and 2.5 μg/mL), plant rhizome extract (10, 25, 55, 75, 100 μg/mL) and silver nitrate solution (0.2, 0.4, 0.5, 0.6, 0.8, 1 μg/mL) in 1 mL PBS. Various concentrations of Cz-AgNPs (1, 1.6, 1.8, 2, 2.5 and 3 μg/mL), plant rhizome extract (10, 25, 55, 75, 100 μg/mL) and silver nitrate solution (0.2, 0.4, 0.5, 0.6, 0.8, 1 μg/mL) were added to test tubes with 1×10^6 EAC cells and were made upto 1 mL with PBS. The test tubes with cancer cell lines and various drugs were incubated for 3 h at 37 °C. After the incubation period, 100 μL of 1% trypan blue was added to the test tubes and allowed to stand for 2 min. The live (unstained) and dead (stained) cells were counted using haemocytometer to determine the percentage of toxicity and the IC_{50} values. The percentage of toxicity was calculated using the formula,

$$Percentage\ of\ cytotoxicity\ =\ \frac{No.\ of\ dead\ cells}{No.\ of\ live\ cells+No.\ of\ dead\ cells}\times100.$$

2.8 Statistical Analysis

The experimental data is expressed as mean ± standard deviation ($n=3$) for each sample using SPSS (version 21) software. The graphs were plotted using Sigma Plot 12.3 software.

3 Results and Discussions

3.1 Green Synthesis of Cz-AgNPs

Upon addition of rhizome extract of *C. zanthorrhiza* to 1 mM silver nitrate solution, an immediate change in the color of the solution was observed. A color change from yellow to light brown and to dark brown was observed as the reaction progressed under sunlight for 1 h (Fig. 1b, c).

The color change indicated the formation of silver nanoparticles at pH = 5.65. The change in color could be attributed to the excitation of surface vibration plasmon in the silver nanoparticles [49]. A preview of literature suggested that the formation of nanoparticles often depends upon the reaction conditions. In general, the formation of silver nanoparticles required thermal decomposition and incubation of the reaction mixtures at room temperature for 180 min and 15 h respectively [50, 51]. However, in the present study, the formation of AgNPs was observed in 60 min indicating the significance of the plant rhizome extract in the facile and rapid synthesis of Cz-AgNPs.

3.2 Characterization of Cz-AgNPs

3.2.1 UV–Visible Spectroscopy

The formation of silver nanoparticles was analyzed by UV–Visible spectroscopy. From the UV–Visible spectrum, the surface plasmon resonance (SPR) peak of the silver nanoparticles was observed at 416 nm (Fig. 2a) [52, 53]. The broadening of peak in the UV–Visible spectrum indicated the polydisperse nature of the silver nanoparticles in the aqueous suspension [54]. The dark brown color of the solution could be attributed to the SPR of the solution which is generated due to the interaction of electromagnetic field with free conduction electrons [55].

3.2.2 Fourier Transform Infrared (FTIR) Spectroscopy

FTIR analysis was performed to identify the various functional groups of plant extract attached to the silver nanoparticles which were responsible for the synthesis and stabilization of the nanoparticles. The FTIR spectra of both the plant rhizome extract and the Cz-AgNPs are displayed in Fig. 2b. The IR spectrum of the plant rhizome extract showed absorption bands at 3467.55 cm^{-1}, 2075.13 cm^{-1}, 1643.13 cm^{-1}, 1074.20 cm^{-1} and 557.25 cm^{-1}. These bands could be assigned to phenolic OH group, C=O stretching vibrations, NH bond of amine group, CO stretching, and CH bending of alkynes respectively [31, 56, 57]. The characteristic absorption bands of Cz-AgNPs were observed at 3448.27 cm^{-1}, 2057.78 cm^{-1}, 1637.35 cm^{-1}, 1049.14 cm^{-1} and 541.92 cm^{-1}. The large shift observed in the absorption bands of the Cz-AgNPs indicated the capping of phytoconstituents in the plant rhizome extract onto the as-synthesized silver nanoparticles. The capping of active molecules on the nanoparticles masks the extreme toxicity found in synthetic nanoparticles. It also enhances the synergistic activity of plant derived secondary metabolites and nanoparticles. The stability of the silver nanoparticles in aqueous medium was probably due to the amide linkage of proteins with Cz-AgNPs [58].

3.2.3 X-Ray Diffraction (XRD) Analysis

The XRD pattern of Cz-AgNPs is depicted in Fig. 3. The well-defined characteristic Bragg's reflection peaks of face centred cubic structure of the metallic silver were observed at 2θ values 38.14°, 46.19°, 64.53° and 77.44° corresponding to the Miller Indices of (111), (200), (222) and (311) planes respectively [59]. The obtained results were found to be in good agreement with JCPDS No. 00-004-0783 indicating the formation of face centred
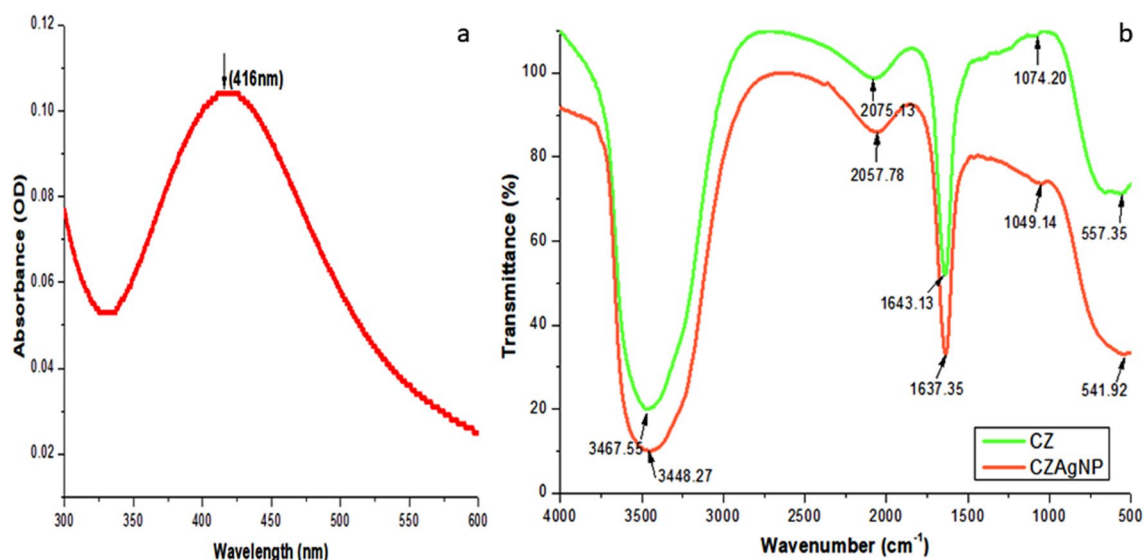

Fig. 2 **a** UV–Visible absorption spectra of Cz-AgNPs with λ $_{max}$ = 416 nm at pH 5.65, **b** FTIR spectrum of the plant rhizome extract (Cz) and synthesized Cz-AgNPs
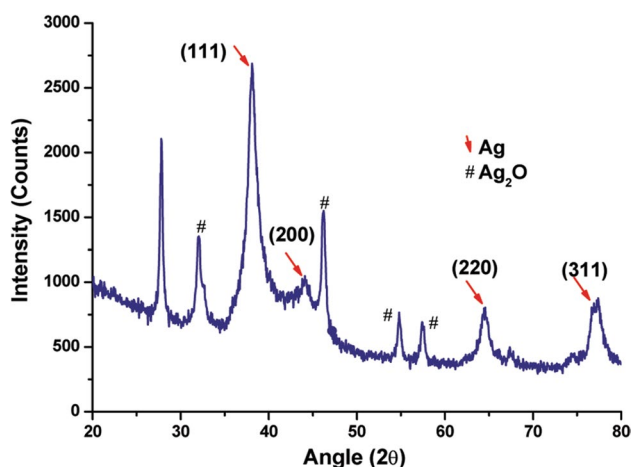
Fig. 3 PXRD pattern of Cz-AgNPs with well characterized Bragg's Reflection peaks at (111), (200), (220) and (311) planes attributing to fcc structure with average crystallite size 17.278 nm

cubic silver. In contrast to the other planes, the intense peak at (111) plane could specify the direction of growth of the synthesized silver nanoparticles [30]. The crystallite size of the silver nanoparticles was determined using Scherrer equation and the average crystallite size of the Cz-AgNPs was found to be 17.278 nm. In addition, four weak peaks corresponding to the silver oxide nanoparticles were observed at 32.23°, 46.10°, 54.57° and 57.39° (JCPDS No. 76-1393). Another peak at 27.82° could be correlated to the silver chloride nanoparticle (JCPDS No. 31-1238).

3.2.4 Electron Microscopy

The size and morphology of the as-synthesized nanoparticles were determined by HR-TEM and FESEM. The HR-TEM images revealed that the Cz-AgNPs were spherical and crystalline in nature. The d-spacing of 0.236 nm was observed
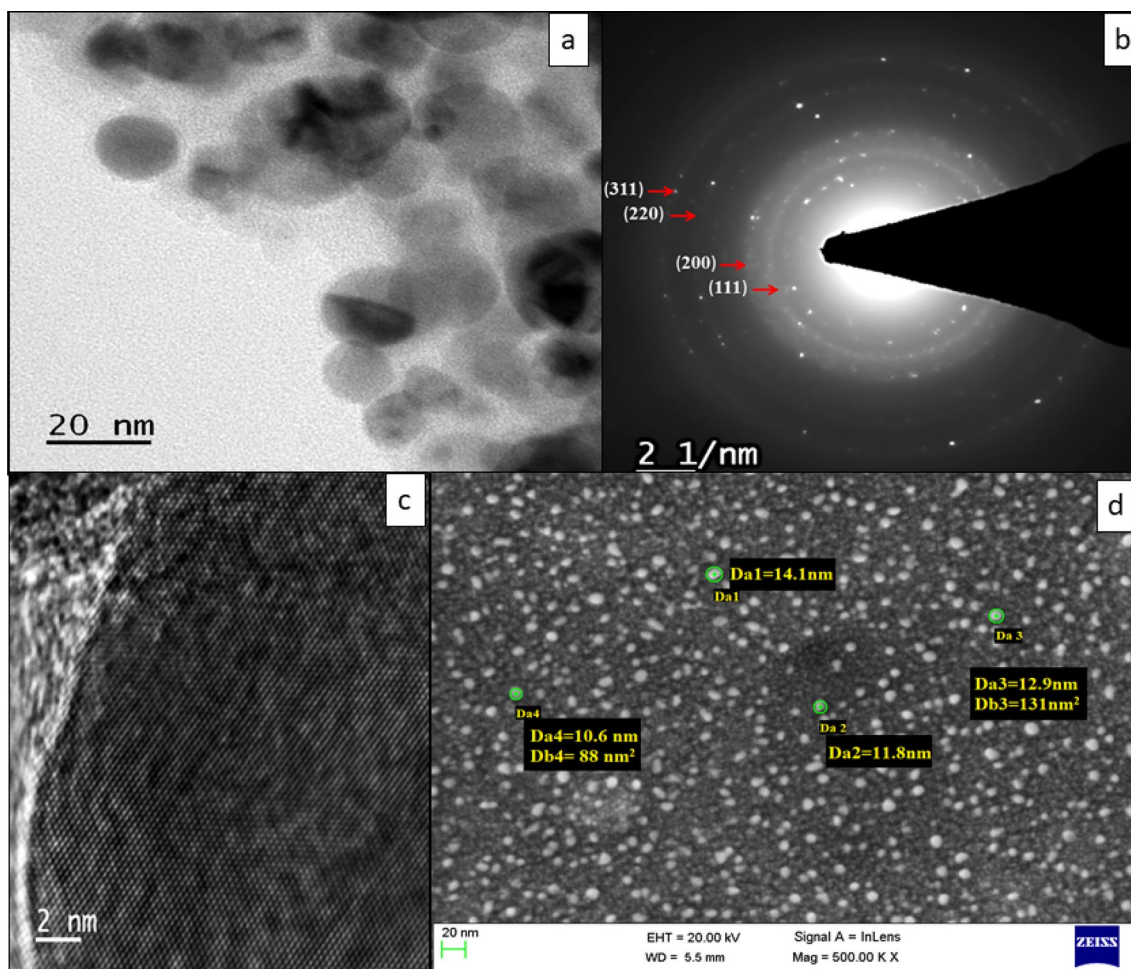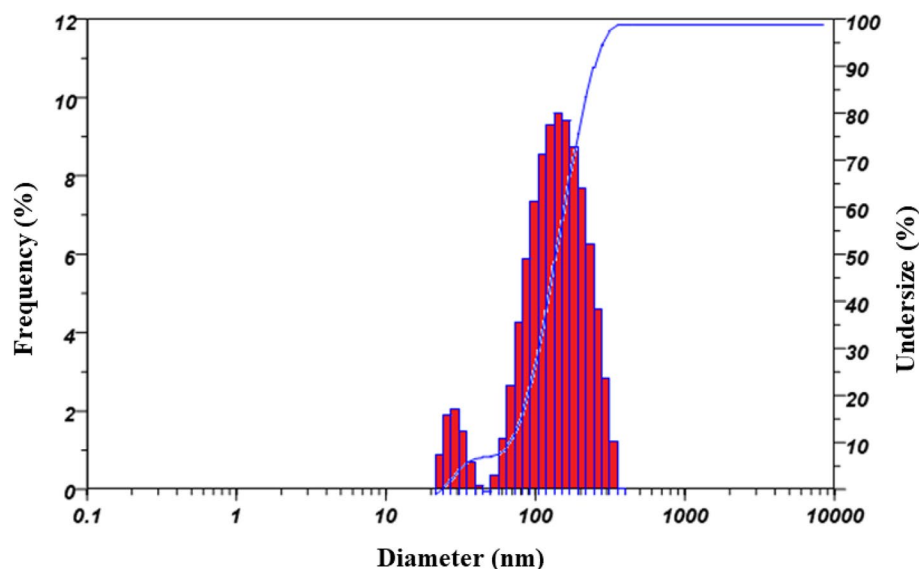

Fig. 4 a HR-TEM image revealing the spherical nature of Cz-AgNPs, **b** SAED pattern of Cz-AgNPs indicating polycrystalline nature with planes coherent to PXRD pattern, **c** HR-TEM image with lattice fringes (d- spacing), **d** FESEM micrograph depicting the spherical morphology of Cz-AgNPs

Fig. 5 Hydrodynamic particle size distribution of Cz-AgNPs measured by DLS analysis

for (111) orientation. The value was in good agreement with that reported for free silver centers ($d_{111} = 0.2359$ nm) (Fig. 4a). The value is hardly distinguishable from Soman and Ray [59] who have obtained a d-spacing value of 0.235 nm for the silver nanoparticles synthesized in this regard. Further the polycrystalline nature of the Cz-AgNPs was revealed from the bright circular spots in the SAED pattern indicating the (111), (200) and (220) planes which were consistent with the obtained XRD pattern (Fig. 4b, c). Moreover, the FESEM micrographs also revealed the spherical morphology of the as-synthesized Cz-AgNPs (Fig. 4d). The average particle size of the Cz-AgNPs was found to be ranging from 10.6 to 15.31 nm.

3.2.5 Dynamic Light Scattering (DLS) Analysis

The DLS results obtained for Cz-AgNPs are shown in Fig. 5. It is observed that the size distribution of Cz-AgNPs ranges from 20 to 145 nm with a Z-average of 111.2 nm and a polydispersity index of 0.348. The size of the Cz-AgNPs obtained from DLS is larger compared to the electron microscopic analysis. The difference in the size of the as-synthesized nanoparticles is due to the influence of Brownian motion [60]. Moreover, this disparity in size could be possibly due to the capping of plant metabolites and adsorption of water on to the as-synthesized silver nanoparticles [33].

3.2.6 BET Surface Analysis

The Nitrogen adsorption—desorption isotherm of Cz-AgNPs were measured using volumetric gas adsorption analyzer. The Nitrogen sorption isotherm of Cz-AgNPs is depicted in Fig. 6. It shows the as-synthesized nanoparticle presents typical IV adsorption. It can be seen from the
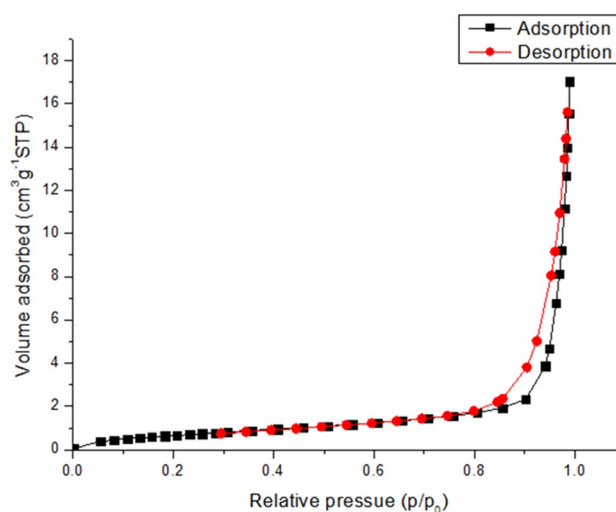

Fig. 6 Nitrogen adsorption–desorption isotherms of Cz-AgNPs

figure, at relative low pressure, the isotherm are flat, which describes the adsorption of Cz-AgNPs mostly occurs in the mesopores. The rapid increase in isotherms and formation of lag loop at relatively high pressure is due to capillary agglomeration phenomenon [61].

From the multipoint BET equation, the calculated specific surface are of Cz-AgNP is 2.683 m^2/g and monolayer adsorption volume is 0.614 cm^3/g (Fig. 7). The cumulative pore volume and pore diameter from the BJH size distribution were found to be 2.634 cm^3 and 39.213 nm respectively. The results ascertained that the as-synthesized nanoparticles are porous with mesoporous nature.
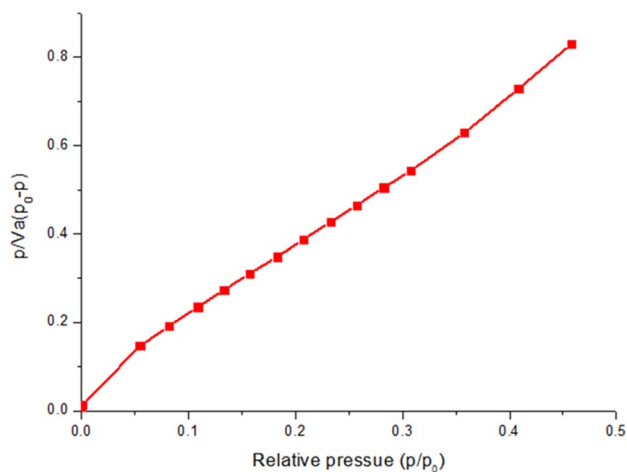
Fig. 7 BET plots of as-synthesized silver nanoparticles at 77 °C

Table 1 Zone of inhibition of various test solutions against bacterial strains (disc diffusion method)

Drug (concentration)	Zone of inhibition (mm)	
	E. coli	S. aureus
Vancomycin (30 mcg)	9.5 ± 0.5	14.9 ± 0.1
Distilled water (control)	Nil	Nil
Cz-AgNPs (100 µg/mL)	8.95 ± 0.05	7.00 ± 0.1
Cz-AgNPs (75 µg/mL)	7.96 ± 0.05	3.9 ± 0.1
Cz-AgNPs (50 µg/mL)	8.00 ± 0	3.83 ± 0.12
Cz-AgNPs (25 µg/mL)	5.93 ± 0.05	3.03 ± 0.15
Cz-AgNPs (10 µg/mL)	4.90 ± 0.1	2.10 ± 0.1
AgNO$_3$ solution (1 mM)	2.00 ± 0.1	1.33 ± 0.15
Plant rhizome extract (0.1 g/mL)	Nil	1.00 ± 0.10

Values are expressed as Mean $\pm$ SD; n $=3$

3.3 Antimicrobial Activity of Cz-AgNPs

3.3.1 Disc Diffusion Method

In disc diffusion assay, the as-synthesized Cz-AgNPs displayed an efficient inhibitory activity against *E. coli* and *S. aureus*. The highest ZOI at 100 µg/mL concentration of Cz-AgNPs was 8.95 ± 0.05 mm and 7 ± 0.1 mm respectively for *E. coli* and *S. aureus*. However, concentration in the range of 10 µg/mL to 75 µg/mL also showed slight inhibition in bacterial growth. The silver nitrate solution and plant rhizome extract alone exhibited negligible activity against the selected bacterial strains. The vancomycin disc exhibited 9.5 ± 0.5 mm and 14.9 ± 0.1 mm ZOI against *E. coli* and *S. aureus* respectively (Table 1).

3.3.2 Broth Microdilution Assay

The Broth microdilution assay explains the MIC of the as-synthesized Cz-AgNPs against two strains of bacteria. After 24 h of incubation, the wells with no color change were scored for the MIC value and the wells stained with dark red color showed the presence of bacteria. The MIC was found to be 4 µg/mL and 32 µg/mL respectively for ampicillin and Cz-AgNPs against *S. aureus.* In the case of *E. coli*, the MIC was 16 µg/mL and 64 µg/mL for the antibiotic ampicillin and Cz-AgNPs. The plant rhizome extract showed the least activity against both the bacterial strains in which the MIC was 512 µg/mL. The MIC of silver nitrate solution was 64 µg/mL for both the bacterial isolates (Fig. 8).

The possible mechanism of antibacterial activity can be attributed to the ultra-small size. And the increased surface to the volume ratio of the nanoparticles which can destroy the membrane, cross the body of the microbe. It can result in ROS generation and finally intracellular damage [62]. It has been observed that size, concentration and shape of the silver nanoparticle can affect its anti-microbial activity. It was found that *E. coli* responded best to triangular-shaped nanoparticles compared to spherical and rod-shaped ones as the triangular shape provides more positive charge to the nanoparticles, ensuring greater antibacterial activity [63]. Therefore, almost equal ZOI exhibited by the Cz-AgNPs and vancomycin for *E. coli* could be attributed to the spherical nature of the as-synthesized nanoparticles rather than triangular nature and also the less surface area of the nanoparticles which was ascertained from nitrogen physisorption. The decrease in ZOI exhibited by Cz-AgNPs in gram-positive bacteria *S. aureus* is perhaps due to the complexity in the composition of the cell wall, which hinders the anchoring of silver nanoparticles onto the bacterial cell wall, thereby obstructing the antibacterial activity [62]. Several researchers have reported the potential of biosynthesized AgNPs as efficient microbicides against various clinical isolates [15, 16]. Novel reports ascertain the resistance of certain bacterial strains to biosynthesized silver nanoparticles. A study by Aina et al. has reported that the efficacy of biosynthesized silver nanoparticles against *S. aureus* and *E. coli* was low even at a concentration 100 µg/mL [28]. This resistance in bacterial strains was due to the repeated exposure of silver nanoparticles buds from the production of flagellin. Flagellin is an adhesive protein, which triggers the agglomeration of nanoparticle, reduces their stability and thereby bring down the efficacy of silver nanoparticles as bactericides [64]. However, the results indicated that the Cz-AgNPs were relatively effective against *E. coli* than to *S. aureus*.

Fig. 8 MIC of Ampicillin (Ab), Cz-AgNPs, plant rhizome extract (PE) and AgNO$_3$ solution respectively against **a** *E. coli* and **b** *S. aureus*. (arrows represent MIC of respective drugs)
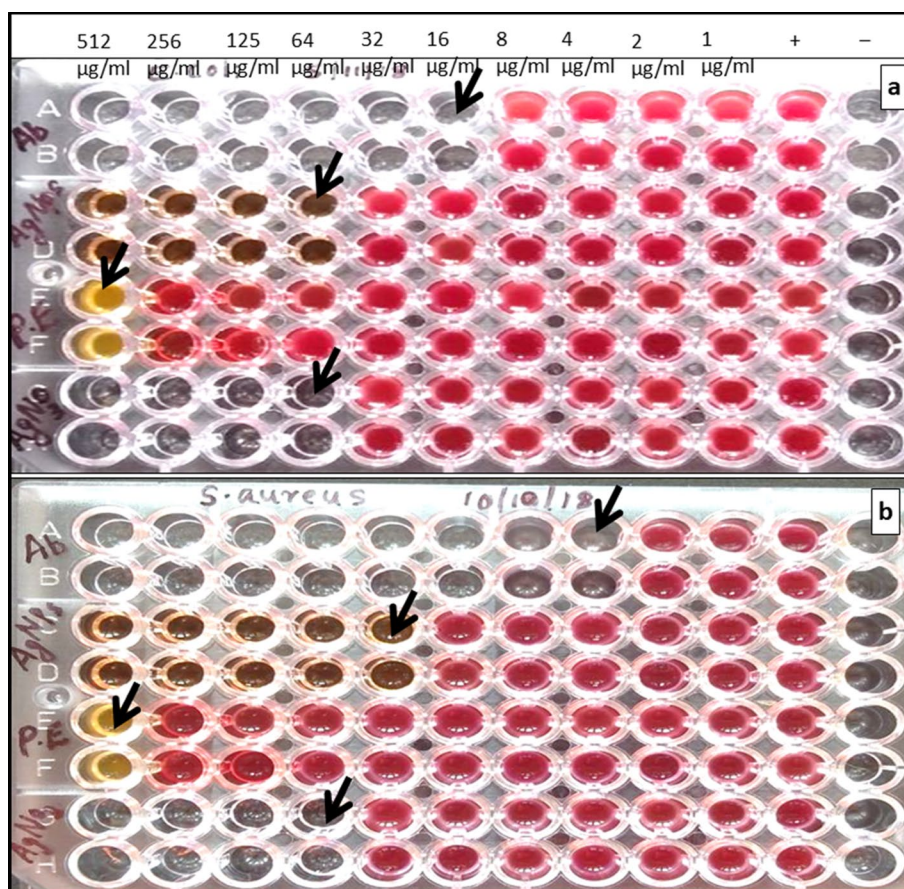

Table 2 Percentage of mycelial growth inhibition by various drugs against fungal pathogen *A. niger*

Drug (concentration)	Mycelial growth (mm)	Percentage of inhibition $=C-T/C\times100$ (%)
Flucanazole (100 µg/mL)	16.50 ± 0.50	80.96
Distilled water (control)	86.66 ± 0.57	0
Cz-AgNPs (100 µg/mL)	11.83 ± 0.76	86.34
Cz-AgNPs (75 µg/mL)	30.00 ± 1.73	65.38
Cz-AgNPs (50 µg/mL)	34.00 ± 1.00	60.76
Cz-AgNPs (25 µg/mL)	35.66 ± 2.08	58.85
AgNO$_3$ solution (1 mM)	47.66 ± 1.15	45.00
Plant rhizome extract (0.1 g/mL)	65.33 ± 3.78	24.61

Values are expressed as mean ± SD; n = 3

3.4 Antifungal Activity of Cz-AgNPs

The antifungal activity of various concentrations of Cz-AgNPs against *A. niger* is presented in Table 2. The rate of fungal growth inhibition was proportional to the concentration of Cz-AgNPs. The standard drug, fluconazole, inhibited 80.96% of fungal growth. The inhibition percentage of silver nitrate solution and plant rhizome extract against *A.* *niger* was 45% and 24.61% respectively, whereas Cz-AgNPs showed 86.34% inhibition at a concentration of 100 µg/mL. Hence, the proliferation of *A. niger* was largely suppressed at a concentration of 100 µg/mL Cz-AgNPs, while the silver nitrate solution and the plant rhizome extract showed very low inhibition rate under the same concentration, demonstrating the antifungal activity of as-synthesized silver nanoparticles. The control group did not show any zone

Table 3 Hemolysis percentage of Cz-AgNPs and silver nitrate solution in the blood stream

Drug (concentration)	Percentage of hemolysis (%)		
	2 h Incubation	4 h Incubation	6 h Incubation
Cz-AgNPs			
2 µg/ml	0.02	0.09	0.15
10 µg/ml	0.06	0.20	0.39
50 µg/ml	0.10	0.24	0.52
100 µg/ml	0.12	0.38	0.81
200 µg/ml	0.20	0.52	1.22
AgNO$_3$ solution (1 mM)	89	92	96

$$\text{Hemolysis percentage} = \left(\text{Absorbance}_{(test)} - \text{Absorbance}_{(negative\ control)}\right) / \left(\text{Absorbance}_{(positive\ control)} - \text{Absorbance}_{(negative\ control)}\right) \times 100\ \%$$

of inhibition. However, the antifungal activity of the metal nanoparticles depends on the size of the nanoparticles as well as on the type of fungus and the deformation of the fungal hyphae may be due to the membrane disintegrity [65]. Nevertheless, the as-synthesized silver nanoparticles have caused detrimental effects to the infectious filamentous fungi *A. niger* manifesting its efficacy in the development of potent antifungal agent. This might be due to the synergistic activity of the Cz-AgNPs formed by the capping of plant rhizome extract.
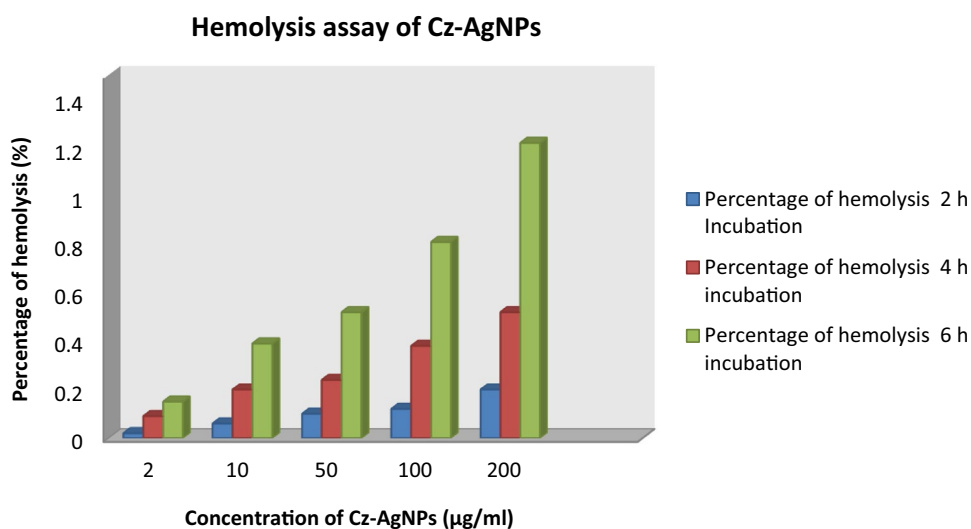
3.5 Hemolysis Assay of Cz-AgNPs

Nanomaterials should be biocompatible for them to be used for pharmaceutical purposes. One of the accepted methods to study biocompatibility is the hemolysis assay [66]. The biocompatibility of Cz-AgNPs was assessed in human RBCs

collected from healthy volunteers. The hemolytic activity was evaluated after 2 h, 4 h and 6 h of incubation. It was found that rate of hemolysis depends on concentration of test solution and the time of incubation (Table 3; Graph 1 and Fig. 9).

The results indicated that less than 1.5% hemolysis occurred in Cz-AgNPs treated groups even after 6 h of incubation, which was very close to PBS (negative control), whereas silver nitrate solution and Triton X (positive control) treated group exhibited 96% and 100% hemolysis respectively. According to ASTME2524-08 standard, the acceptable blood damage criterion is below 5% [67]. Earlier research reports have shown that under optimal conditions green synthesized nanoparticles were biocompatible [58, 59]. The smallest sized silver nanoparticles displayed greater ability to induce membrane damage due to the direct interaction between RBC and nanoparticles. It results in stress and afterwards hemolysis [68]. Though, the present results stand well within the standard limits of biocompatibility, further studies are required before using the as-synthesized Cz-AgNPs for bioimaging and drug delivery.

3.6 In Vitro Cytotoxicity Assay of Cz-AgNPs

The short term in vitro cytotoxicity of Cz-AgNPs was compared with plant rhizome extract and silver nitrate solution using trypan blue exclusion method in DLA and EAC cell lines. The transparent viable cells and stained dead cells were counted using hemocytometer. The percentage cytotoxicity exhibited by the Cz-AgNPs, plant rhizome extract and silver nitrate solution on DLA and EAC cell lines are presented in Tables 4, 5. The plant rhizome extract, Cz-AgNPs and silver nitrate solution exhibited a dose-dependent cell death in both DLA and EAC cell lines. The IC 50 value of the plant rhizome extract,

Graph 1 Representation of hemolysis assay of green synthesized Cz-AgNPs
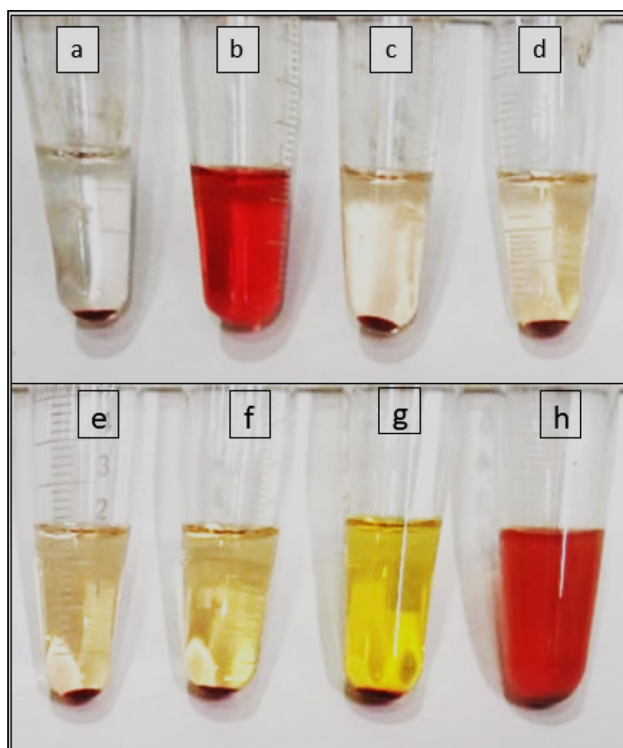
Fig. 9 Hemolysis activity **a** PBS, **b** Triton-X, **c** 2 µg/ml, **d–g** Cz-AgNPs at 10 µg/ml, 50 µg/ml, 100 µg/ml, 200 µg/ml concentrations respectively and **h** AgNO₃ solution

Table 4 Comparison of percentage cytotoxicity of Cz-AgNPs, plant rhizome extract and silver nitrate solution against DLA cell lines

Drug	Concentration (µg/mL)	Percentage cytotoxicity (%)	IC$_{50}$ value (µg/mL)
Cz-AgNPs	0.2	2.42	1.67
	0.6	6.95	
	0.8	13.65	
	1.0	18.74	
	1.6	34.17	
	2.5	93.75	
AgNO₃ solution	0.2	6.91	0.494
	0.4	13.34	
	0.5	53.94	
	0.6	76.74	
	0.8	83.2	
	1	95.68	
Plant rhizome extract	10	4.42	90.13
	25	7.62	
	35	19.41	
	55	21.15	
	75	42.35	
	100	62.5	

Percentage of cytotoxicity $= \frac{\text{No. of dead cells}}{\text{No. of live cells} + \text{No. of dead cells}} \times 100$

Table 5 Comparison of percentage cytotoxicity of Cz-AgNPs, plant rhizome extract and silver nitrate solution against EAC cell lines

Drug	Concentration (µg/mL)	Percentage cytotoxicity (%)	IC$_{50}$ value (µg/mL)
Cz-AgNPs	1.0	14.39	1.84
	1.6	23.48	
	1.8	35.28	
	2.0	53.30	
	2.5	83.87	
	3.0	91.4	
AgNO₃ solution	0.2	7.66	0.513
	0.4	49.40	
	0.5	63.10	
	0.6	70.46	
	0.8	78.85	
	1	80.34	
Plant rhizome extract	10	17.17	50.23
	25	15.42	
	35	33.78	
	55	41.24	
	75	79.3	
	100	96.34	

Percentage of cytotoxicity $= \frac{\text{No. of dead cells}}{\text{No. of live cells} + \text{No. of dead cells}} \times 100$

Cz-AgNPs and silver nitrate solution in DLA cells was determined to be 90.13 µg/mL, 1.67 µg/mL and 0.494 µg/mL respectively. In EAC cell lines the IC 50 value was observed to be 50.23 µg/mL, 1.84 µg/mL and 0.513 µg/mL for the plant rhizome extract, Cz-AgNPs and silver nitrate solution respectively. It has been reported that 200 µg/mL of silver nanoparticles synthesized using *F. hispida* leaf extracts, *Colpomenia sinuosa* and *Halymenia poryphyroides* completely inhibits DLA and EAC cells [55, 69]. Kanagamani et al. [70] reported that 50 µg/mL of standard drug curcumin is required for 98.07% of inhibition of DLA cells. Interestingly, in our study 2.5 µg/mL and 3 µg/mL of silver nanoparticles synthesized using rhizome extract of *C. zanthorrhiza* inhibited 97.99% of DLA cells and 91.4% of EAC cells respectively. This finding validates that low doses of Cz-AgNPs can effectively inhibit the viability and proliferation of DLA and EAC cell lines.

The silver nanoparticles were found to inhibit the cell cycle by generating ROS resulting in the death of the cancer cells [71]. Many reports show that silver nanoparticles are effective against various cancer cell lines like MCF 7 (breast cancer) cells [72], Hep G2 cell lines of liver cancer [73]. However, in vivo experiments are to be performed before clinical trials and the development of new formulations of silver nanoparticles against tumor cell lines.

4 Conclusion

The green synthesis of AgNPs using *C. zanthorrhiza* aqueous rhizome extract has been reported the first time via photo-mediated process. The synthesis of Cz-AgNPs was confirmed using UV–Visible Spectroscopy with a Surface Plasmon Resonance band at 416 nm. PXRD pattern revealed the face centred cubic crystal structure of Cz-AgNPs with an average crystallite size of 17 nm. FTIR analysis demonstrated the efficient capping of plant derived phytoconstituents onto the Cz-AgNPs. HR-TEM and FESEM micrographs showed the spherical crystalline nature of Cz-AgNPs. The BET analaysis revealed mesoporous nature of Cz-AgNPs. The results indicated that Cz-AgNPs can be used as antimicrobial agents against human pathogenic bacteria and plant pathogenic fungi. The present study also revealed the effects of as-synthesized Cz-AgNPs on anticancer activities by effectively inhibiting the viability and proliferation of DLA and EAC cell lines. The biocompatible nature of Cz-AgNPs was investigated by the hemolysis assay of human erythrocytes. The results are promising as they can contribute to the upgraded utilization of Cz-AgNPs for drug delivery and for therapeutic drug development.

Compliance with Ethical Standards

Conflict of interest The authors have no conflicts of interest to declare that are relevant to the content of this article.

References

1. N. Norouzi, M.K. Das, A.J. Richard, A.A. Ibrahim, H.M. El-Kaderi, S. El-Shall, Nanoscale **12**, 19191 (2020)
2. P. Prosposito, L. Burratti, I. Venditti, Chemosensors **8**, 1 (2020)
3. M. Gisbert-Garzarán, J.C. Berkmann, D. Giasafaki, D. Lozano, K. Spyrou, M. Manzano, T. Steriotis, G.N. Duda, K. Schmidt-Bleek, G. Charalambopoulou, M. Vallet-Regí, A.C.S. Appl, Mater. Interfaces **12**, 14946 (2020)
4. F. Ren, H. Liu, H. Zhang, Z. Jiang, B. Xia, C. Genevois, T. He, M. Allix, Q. Sun, Z. Li, M. Gao, Nano Today **34**, 100905 (2020)
5. K.D. Lee, P.C. Nagajyothi, J. Nanomater. **2011**, 557 (2011)
6. P.B. Dayma, A.V. Mangrola, S.P. Suriyaraj, P. Dudhagara, K. Rajesh, J. Pharm. Chem. Biol. Sci. **7**, 94 (2019)
7. S.E. Cross, Y.S. Jin, Q.Y. Lu, J. Rao, J.K. Gimzewski, Nanotechnology **22**, 215101 (2011)
8. S. Quideau, D. Deffieux, C. Douat-Casassus, L. Pouységu, Angew. Chem. - Int. Ed. **50**, 586 (2011)
9. O. OoKolawole, S. Oguntoye, O. Agbede, A. Olayemi, Ethnobot. Leafl. **10**, 228 (2006)
10. A.R. Bilia, V. Piazzini, C. Guccione, L. Risaliti, M. Asprea, G. Capecchi, M.C. Bergonzi, Planta Med. **83**, 366 (2017)
11. C.L. Criado, J. Nanomed. Res. **2**, 2 (2015)
12. M. Ovais, A.T. Khalil, A. Raza, M.A. Khan, I. Ahmad, N.U. Islam, M. Saravanan, M.F. Ubaid, M. Ali, Z.K. Shinwari, Nanomedicine **12**, 3157 (2016)
13. R. Sankar, P.K.S.M. Rahman, K. Varunkumar, C. Anusha, A. Kalaiarasi, K.S. Shivashangari, V. Ravikumar, J. Mol. Struct. **1129**, 8 (2017)
14. X.F. Zhang, Z.G. Liu, W. Shen, S. Gurunathan, Int. J. Mol. Sci. **17**, 1534 (2016)
15. V. Castro-aceituno, V. Castro-aceituno, S. Ahn, S. Yesmin, P. Singh, Biomed. Pharmacother. **84**, 158 (2017)
16. A.K.M.R. Uddin, M.A.B. Siddique, F. Rahman, A.K.M.A. Ullah, R. Khan, J. Inorg. Organomet. Polym. Mater. **30**, 3305 (2020)
17. S. Ghojavand, M. Madani, J. Karimi, J. Inorg. Organomet. Polym. Mater. **30**, 2987 (2020)
18. U.R. Shwetha, M.S. Latha, C.R. Rajith Kumar, M.S. Kiran, V.S. Betageri, J. Inorg. Organomet. Polym. Mater. (2020). https://doi.org/10.1007/s10904-020-01575-w
19. M.S. Kiran, V.S. Betageri, C.R.R. Kumar, S.P. Vinay, M.S. Latha, J. Inorg. Organomet. Polym. Mater. **30**, 2916 (2020)
20. G. Das, J.K. Patra, T. Debnath, A. Ansari, H.S. Shin, PLoS ONE **14**, 1 (2019)
21. L.P. Silva, T.M. Pereira, C.C. Bonatto, *Frontiers and Perspectives in the Green Synthesis of Silver Nanoparticles* (Elsevier Inc., Amsterdam, 2019).
22. N.A. Ramos-Delgado, L. Hinojosa-Reyes, I.L. Guzman-Mar, M.A. Gracia-Pinilla, A. Hernández-Ramírez, Catal. Today **209**, 35 (2013)
23. U. Kamran, H.N. Bhatti, M. Iqbal, S. Jamil, M. Zahid, J. Mol. Struct. **1179**, 532 (2019)
24. K.B.A. Ahmed, R. Senthilnathan, S. Megarajan, V. Anbazhagan, J. Photochem. Photobiol. B **151**, 39 (2015)
25. S. Yari, S. Abbasizadeh, S.E. Mousavi, M.S. Moghaddam, A.Z. Moghaddam, Process Saf. Environ. Prot. **94**, 159 (2015)
26. P. Nasehi, B. Mahmoudi, S.F. Abbaspour, M.S. Moghaddam, RSC Adv. **9**, 20087 (2019)
27. P. Nasehi, M.S. Moghaddam, S.F. Abbaspour, N. Karachi, Sep. Sci. Technol. **55**, 1078 (2020)
28. D.A. Aina, O. Owolo, A. Lateef, F.O. Aina, A.S. Hakeem, Karbala Int. J. Mod. Sci. **5**, 2 (2019)
29. S. Arokiyaraj, S. Vincent, M. Saravanan, Y. Lee, Y.K. Oh, K.H. Kim, Artif. Cells Nanomed Biotechnol. **45**, 372 (2017)
30. A.V. Ramesh, D.R. Devi, G.R. Battu, K. Basavaiah, S. Afr. J. Chem. Eng. **26**, 25 (2018)
31. O.T. Jemilugba, E.H.M. Sakho, S. Parani, V. Mavumengwana, O.S. Oluwafemi, Colloids Interface Sci. Commun. **31**, 100191 (2019)
32. S. Some, O. Bulut, K. Biswas, A. Kumar, A. Roy, I.K. Sen, A. Mandal, O.L. Franco, İA. İnce, K. Neog, S. Das, S. Pradhan, S. Dutta, D. Bhattacharjya, S. Saha, P.K. Das Mohapatra, A. Bhuimali, B.G. Unni, A. Kati, A.K. Mandal, M.D. Yilmaz, I. Ocsoy, Sci. Rep. **9**, 1 (2019)
33. B. Rao, R.C. Tang, Adv. Nat. Sci. Nanosci. Nanotechnol. **8**, 015014 (2017)
34. A.R.M. Abd El-Aziz, M.R. Al-Othman, Pak. J. Bot. **51**, 443 (2019)
35. M. Srinivasan, M. Venkatesan, V. Arumugam, G. Natesan, N. Saravanan, S. Murugesan, S. Ramachandran, R. Ayyasamy, A. Pugazhendhi, Process Biochem. **80**, 197 (2019)
36. T. Rasheed, F. Nabeel, M. Bilal, H.M.N. Iqbal, Biocatal. Agric. Biotechnol. **19**, 101154 (2019)

37. A.O. Nyabola, P.G. Kareru, E.S. Madivoli, S.I. Wanakai, E.G. Maina, J. Inorg. Organomet. Polym. Mater. **30**, 3493 (2020)
38. P. Moteriya, S. Chanda, J. Inorg. Organomet. Polym. Mater. **30**, 3920 (2020)
39. A.G. Rama Krishna, C.S. Espenti, Y.V. Rami Reddy, A. Obbu, M.V. Satyanarayana, J. Inorg. Organomet. Polym. Mater. **30**, 4155 (2020)
40. H.P.A. Mary, G.K. Susheela, S. Jayasree, A.M. Nizzy, B. Rajagopal, S. Jeeva, Asian Pac. J. Trop. Biomed. **2**, S637 (2012)
41. C. Singgih Wahono, C. Diah Setyorini, H. Kalim, N. Nurdiana, K. Handono, Int. J. Rheumatol. (2017). https://doi.org/10.1155/2017/7687053
42. S. Anjusha, A. Gangaprasad, J. Pharmacogn. Phytochem. **3**, 50 (2014)
43. P.N. Ravindran, K. Nirmal Babu, K. Sivaraman, *Turmeric: The Genus Curcuma* (CRC Press, Boca Raton, 2007).
44. A.W. Bauer, W.M.M. Kirby, J.C. Sherris, A.M. Turck, A. Von Graevenitz, Am. J. Clin. Pathol. **45**, 493 (1978)
45. A. Mourey, N. Canillac, Food Control **13**, 289 (2002)
46. J.N. Eloff, Planta Med. **64**, 711 (1998)
47. Y.L. Nene, P.N. Thapliyal, *Fungicides in Plant Disease Control* (Oxford & IBH Publisher house, New Delhi, 1979).
48. Y.S. Lin, C.L. Haynes, J. Am. Chem. Soc. **132**, 4834 (2010)
49. P. Mulvaney, Langmuir **12**, 788 (1996)
50. S.M. Hosseinpour-mashkani, M. Ramezani, Mater. Lett. **130**, 259 (2014)
51. S. Muthukrishnan, B. Vellingiri, G. Murugesan, Futur. J. Pharm. Sci. **4**, 206 (2018)
52. S. Wei, Y. Wang, Z. Tang, J. Hu, R. Su, J. Lin, T. Zhou, H. Guo, N. Wang, R. Xu, New J. Chem. **44**, 9304 (2020)
53. N. Tarannum, Divya, Y.K. Gautam, RSC Adv. **9**, 34926 (2019)
54. S. Bhowmik, B.K. Datta, A.K. Saha, P. Chakma, N.C. Mandal, Not. Sci. Biol. **8**, 106 (2016)
55. K. Kanagamani, P. Muthukrishnan, M. Ilayaraja, K. Shankar, A. Kathiresan, J. Inorg. Organomet. Polym. Mater. **28**, 702 (2018)
56. D. Sasidharan, T.R. Namitha, S.P. Johnson, V. Jose, P. Mathew, Sustain. Chem. Pharm. **16**, 100255 (2020)
57. S. Ojha, A. Sett, U. Bora, Adv. Nat. Sci. Nanosci. Nanotechnol. **8**, 035009 (2017)
58. S. Priyadarshini, V. Gopinath, N. Meera Priyadharsshini, D. MubarakAli, P. Velusamy, Colloid Surf. B **102**, 232 (2013)
59. S. Soman, J.G. Ray, J. Photochem. Photobiol. B **163**, 391 (2016)
60. B. Adebayo-Tayo, A. Salaam, A. Ajibade, Heliyon **5**, e02502 (2019)
61. Z. Wei, M. Zhou, H. Qiao, L. Zhu, H. Yang, T. Xia, J. Nanomater. **2009**, 5 (2009)
62. G. Franci, A. Falanga, S. Galdiero, L. Palomba, M. Rai, G. Morelli, M. Galdiero, Molecules **20**, 8856 (2015)
63. S. Pal, Y.K. Tak, J.M. Song, Appl. Environ. Microbiol. **73**, 1712 (2007)
64. A. Panáček, L. Kvítek, M. Smékalová, R. Večeřová, M. Kolář, M. Röderová, F. Dyčka, M. Šebela, R. Prucek, O. Tomanec, R. Zbořil, Nat. Nanotechnol. **13**, 65 (2018)
65. S. Medda, A. Hajra, U. Dey, P. Bose, N.K. Mondal, Appl. Nanosci. **5**, 875 (2015)
66. A. Mayer, M. Vadon, B. Rinner, A. Novak, R. Wintersteiger, E. Fröhlich, Toxicology **258**, 139 (2009)
67. J. Choi, V. Reipa, V.M. Hitchins, P.L. Goering, R.A. Malinauskas, Toxicol. Sci. **123**, 133 (2011)
68. L.Q. Chen, L. Fang, J. Ling, C.Z. Ding, B. Kang, C.Z. Huang, Chem. Res. Toxicol. **28**, 501 (2015)
69. D.M.S. Vishnu Kiran Manam, World J. Pharm. Sci. **2**, 926 (2014)
70. K. Kanagamani, P. Muthukrishnan, K. Shankar, A. Kathiresan, H. Barabadi, M. Saravanan, J. Clust. Sci. **30**, 1415 (2019)
71. S.P. Singh, A. Mishra, R.K. Shyanti, R.P. Singh, A. Acharya, Biol. Trace Elem. Res. (2020). https://doi.org/10.1007/s12011-020-02255-z
72. R.R. Remya, S.R.R. Rajasree, L. Aranganathan, T.Y. Suman, Biotechnol. Rep. **8**, 110 (2015)
73. M. Sivakumar, S. Surendar, M. Jayakumar, P. Seedevi, P. Sivasankar, M. Ravikumar, M. Anbazhagan, T. Murugan, S.S. Siddiqui, S. Loganathan, J. Clust. Sci. **32**, 167–177 (2020)